INTERNATIONAL JOURNAL FOR NUMERICAL METHODS IN FLUIDS, VOL. 7, 833–855 (1987)

AN OCEAN MODELLING SYSTEM WITH TURBULENT BOUNDARY LAYERS AND TOPOGRAPHY: NUMERICAL DESCRIPTION

DAVID E. DIETRICH AND M. G. MARIETTA

Sandia National Laboratories, Albuquerque, NM 87185, U.S.A.

AND

PATRICK J. ROACHE

Ecodynamics Research Associates, P.O. Box 8172, Albuquerque, NM 87198, U.S.A.

SUMMARY

The Sandia ocean modelling system (SOMS) is a system of three-dimensional, fully conservative, partially implicit numerical models based on primitive equations and a staggered Arakawa 'c' grid. A thin-shell bottom boundary layer submodel coupled to a free-stream submodel resolves boundary layers together with realistic topography. Both submodels use stretched vertical co-ordinates and an optional Mellor–Yamada level-2·5 turbulence closure. Rigid top pressures are determined by vertical integration of the conservation equations using a hydrostatic approximation. SOMS reproduces previously published results, but with notable advantages in speed and economy.

KEY WORDS Pseudo-body-fitted Partially Implicit Conservative Primitive Equations Staggered Grid Turbulent Thin Shell

1. INTRODUCTION

Mathematical computer models are currently being used with relevant observations to assess the transport and dispersion of soluble and suspendable materials originating from bottom sources in the deep ocean.[1,2] For realistic results, ocean models must treat complex phenomena on a range of scales, including basic gyre-scale flow, the mesoscale eddy field, phenomena such as boundary-layer separation associated with bottom topography, and turbulent mixing processes in the bottom boundary layer. Dispersion studies have been done before in idealized quasi-geostrophic regional scale models without boundary layers[3] and with boundary layers.[4] For assessment and monitoring applications such as nuclear waste disposal, real ocean forecasts and simulations must be performed. This requires ocean models that cover the full range of space and time scales and that can assimilate real ocean data.

As described by Marietta and Robinson[1] one approach to this complex modelling problem is to construct a hierarchical series of models by interfacing existing models. The hierarchical series described in Reference 1 consists of a general circulation model[5,6] with an embedded quasigeostrophic regional-scale model.[7,8] Boundary layer[9] and coastal[10] models are interfaced to each of these. This approach, although timely and workable, has a number of difficulties

0271–2091/87/080833–23$11.50

Received 11 August 1986
Revised 8 December 1986

associated with interfacing the different model physics and numerics. The present paper reports on a modelling system that replaces the hierarchy of different types of models. This system provides consistent physics and efficient numerics for important applied problems concerned with a wide range of ocean scales. Although the fundamental momentum, energy, mass and species conservation equations are applicable to the full range of ocean scales, direct application often requires high space and time resolution beyond available and envisioned computing capability in calculating the associated multi-scale interactions. However, it is possible to approximate these processes by using a turbulence closure scheme, which is the approach taken here.

The Sandia ocean modelling system (SOMS) presented here is not just one model, but a modelling methodology to be applied in different modes (coarse or high resolution, boundary layers, with or without realistic topography, in a forecast or phenomenological mode, etc.) according to application requirements; hence its description as a modelling *system*. SOMS is a system of primitive equation numerical models. The master version is three dimensional, and divides the modelled ocean into lower and upper subdomains. The lower subdomain is addressed by a thin-shell bottom boundary layer submodel, and the upper subdomain by a free-stream submodel. The lower is a thin layer of constant thickness that includes the bottom mixed layer, whereas the upper subdomain is the overlying ocean. This coupled system is intended to facilitate efficient modelling of the bottom boundary layer with realistic topography. Coupling is accomplished through continuity conditions applied at the common interface, which is an undulating surface at the top of the thin-shell submodel domain. (The two submodels can also be run separately, or coupled to other appropriate models). The free-stream submodel can address the free-stream flow (with bottom topography) and/or the top boundary layer. To address boundary layer dynamics efficiently and accurately both submodels use a stretched vertical co-ordinate normal to the ocean boundary, and both have an optional Mellor–Yamada level-2·5 turbulence closure scheme with associated subgrid scale turbulence energy and length scale predictive relations (similar to the atmospheric boundary layer[11]). Currently, the thin-shell submodel ignores co-ordinate curvature effects associated with bottom topography, a common boundary layer approximation.

The basic numerical approach is described in section 2. The model finite difference equations are given in section 3. The corresponding continuum equations are given in Appendix I. For model validation and comparison with earlier models, SOMS application to a flat-bottom rectangular-basin idealization of the North Atlantic Ocean is described briefly in section 4 and more completely in Reference 12. Later papers will describe SOMS applications to realistic ocean basins and forecast situations.

2. THE NUMERICAL APPROACH

SOMS includes the following numerical features: it uses coupled thin-shell and free-stream submodels; it treats boundary fluxes numerically as internal sources; it uses a control volume approach with staggered control volumes corresponding to the Arakawa 'c' staggered grid;[13] its numerical contribution in each direction to the diffusion coefficients is based on a user-specified directional cell Reynolds number and, to avoid logical decisions, this contribution is simply added to the user-specified nominal diffusion coefficient and any contribution from a turbulence closure model; it implicitly couples Coriolis and vertical diffusion terms; it uses a modified leap-frog time integration scheme and a Mellor–Yamada level-2·5 turbulence closure scheme.[14] We describe these features in more detail below.

2.1. *Basic considerations*

Since boundary layer separation and mass transport are important in deep dispersion applications, it is important to model advection correctly. Although large-scale flow closely follows isopycnals and is nearly horizontal over most of the ocean, vertical advection is important for dispersion applications. Vertical advection *must* be included in order to have desirable conservation properties and to avoid unphysical results when horizontal advection due to divergent horizontal flow (which occurs in response to topography as well as in Ekman layers) is included. Such conservation is desirable in modelling geophysical flows. Owing to the quasisteady nature and low dissipation rate of geophysical flow features of primary interest, small conservation errors can lead to relatively large time derivative errors and accumulate. Thus, both SOMS submodels (see section 2.2) include both horizontal and vertical advection.

SOMS use of the hydrostatic approximation is described in detail in Appendix II. Non-hydrostatic pressure interaction with topography might also be needed for realistic boundary layer separation modelling, especially for large bottom slopes. At present SOMS does not include such effects, but a possible approach to including them is given in Appendix II.

The SOMS two-model approach uses pseudo-boundary-fitted co-ordinates for efficient treatment of the ocean's undulating bottom boundary layer; the co-ordinates in the lower subdomain actually align with the boundary (bottom topography), but are then patched in a 'staircase' manner to the upper subdomain. Such an approach facilitates fine 'vertical' (normal to the undulating ocean bottom) resolution. It also separates the thin-undulating turbulent boundary layer that is adjacent to the bottom topography from the free ocean. This separation allows the relatively thin boundary layer part of the model to include a good turbulence closure scheme, while avoiding the associated extra computation in the free ocean part of the model if desired. Using a true boundary-fitted co-ordinate system for the total ocean is an attractive alternative, but can result in unnecessarily elaborate calculations in the free ocean where general curvilinear coordinates are not a major advantage.

2.2. *Thin-shell and free stream models*

SOMS uses a thin-shell model (TSM) to predict flow in a thin boundary region adjacent to the topography and a free-stream model (FSM) to predict flow above this thin-shell region. Coupling is accomplished through flux continuity conditions, as described in detail in Appendix III. FSM can either interface to other models, such as a quasigeostrophic model, or model the entire ocean that overlies TSM.

Bottom topography results in an undulating interface between the constant thickness TSM subdomain and the FSM subdomain. In FSM, this interface is simply approximated in a 'staircase' manner by finite difference hatching, in which each FSM control volume is considered either wholly above or wholly below the FSM/TSM interface (Figure 1). The alternative of using boundary-fitted co-ordinates, which would make such an interface a co-ordinate surface, is not an advantage in FSM. The pseudo-boundary-fitted co-ordinates used by TSM allow accurate boundary layer resolution using a stretched (log-linear) 'vertical' co-ordinate (Appendix IV).

At present, boundary layer co-ordinate curvature is ignored in the thin-shell model equations. Boundary layer vertical shears dominate curvature effects, except for flow features whose horizontal scales are not large compared to the boundary layer depth, such as Goertler vortices and small-scale topography effects. Such flow features are sometimes non-hydrostatic, and must be parametrized in a turbulence closure model unless very high resolution is used.

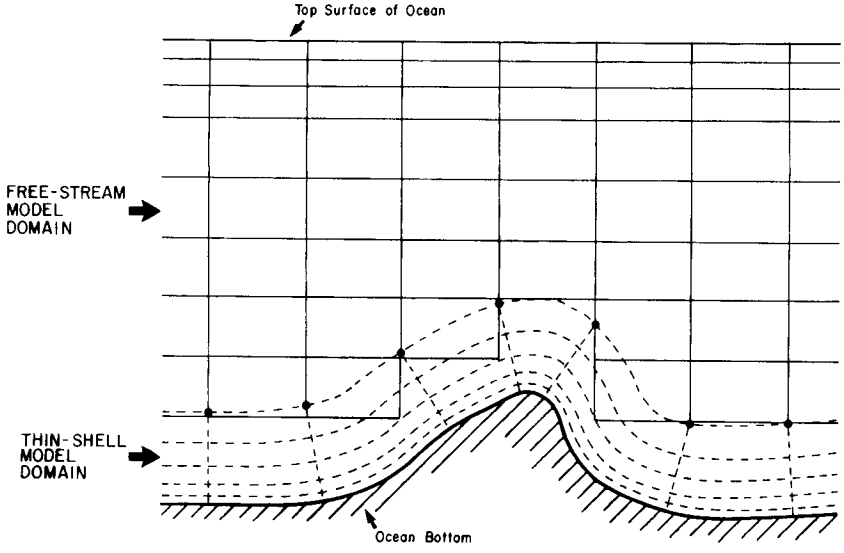

Figure 1. Bottom topography and thin-shell submodel (exaggerated topography). A longitudinal-vertical slab showing control volume boundaries (solid lines for free-stream submodel and dashed lines for thin-shell submodel)

Such boundary curvature can force curved mean flow trajectories in the boundary layer, which can strongly affect the conversion between mean flow kinetic energy and turbulence kinetic energy through the Taylor (centrifugal) instability mechanism (see Goertler vortex theory[15]). Such flow curvature effects are not addressed in the turbulence kinetic energy source term used in the Mellor–Yamada level-2·5 turbulence closure scheme applied in the TSM, nor indeed in most turbulence closure schemes. We will consider possible alternate formulations in the future.

Although the subgrid-scale turbulent eddies that dominate vertical transport in the bottom boundary layer do not interact directly in the TSM with the resolved topography, they do interact with the vertical shear of the mean horizontal velocity which interacts with the resolved topography through the TSM/FSM coupling. Turbulent eddy interaction with *unresolved* topography, if important, can be parametrized. Thus, it is possible to address all direct topographic interactions in FSM (however, see section 5.1).

2.3. *Boundary fluxes treated as sources*

Instead of specifying the usual flux conditions at its hatched bottom boundary, FSM sets zero numerical fluxes, but includes bottom physical effects from TSM numerically as *sources* to the FSM control volumes. This convenient method produces only a local first-order error. The same method is used for user-specified inflows at model ports, which are included as user-specified sources.

This boundary source approach allows convenient treatment of *unresolved* jets that are known to exist on boundaries, such as the Mediterranean inflow at the eastern boundary of the Atlantic Ocean. Most previous models simply specify the mean velocity at the control volume face containing the inflow. In doing this, mass and/or momentum inflow associated with the specified velocity are generally compromised. If the specified velocity reflects the proper mass inflow, the derived momentum inflow will generally be wrong, because the mass inflow is linearly

related to the unresolved jet velocity, whereas the momentum inflow is quadratically related. Thus, the same velocity-averaging scheme cannot be applied for computing both quantities, and one is left with the awkward situation of specifying two different 'average' jet velocities at the inflow. SOMS uses the better method of specifying inflows as boundary sources of mass, energy, momentum and species, as directly required by the conservation equations.

When real subgrid-scale inflow jets are known to penetrate several zones before spreading out to resolved scales, the inflows are represented by appropriately distributing momentum, heat, mass and species sources over several zones according to available jet penetration observations, as part of the total subgrid closure scheme. This 'distributed jet' approach was used in a coal gasifier model[16] and is an option with SOMS.

This source treatment of boundary fluxes is convenient and general, and facilitates program modularization.

2.4. *Staggered control volumes*

The source approach described in section 2.3 is natural when using control volumes. Each cubical finite volume or 'cell' is treated as a 'control volume' in which the conservation equations are applied to the finite volume as a whole.[17] Thus, the time derivatives of the volume-integrated conserved quantity densities (energy, momentum and species, where species refers to any material that is modelled as an independently transported quantity) in each volume are related to corresponding fluxes integrated over the volume boundaries, plus pressure work done on boundaries and species sources within the volumes (such as a bottom source of dispersing material). The fluxes are computed from the instantaneous values of the conserved quantity densities. Flux contributions associated with unresolved space and time fluctuations on the control volume boundaries are determined from the turbulence closure scheme. Interpolations are used as appropriate.

The fundamental control volumes or 'cells' are used for calculating scalar quantities such as pressure, temperature, density and salinity (see Figure 2). Control volumes for mass flux components are centred on scalar cell faces which are normal to the flux component. This corresponds to the widely used Arakawa 'c' staggered grid.[13] The scalar cells are considered either wholly inside or wholly outside the modelled ocean region.

2.5. *Directed diffusion coefficients*

In geophysical flows it is desirable to minimize numerical diffusion, as most of the energy is

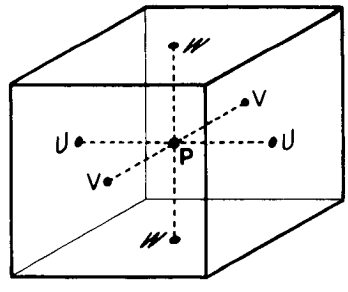

Figure 2. Arakawa 'c' staggered grid: single control volume for pressure (P). The symbol P denotes centre of the P-control volume. The symbols U, V and W illustrate relative positions of control volume centres for longitudinal, latitudinal and vertical velocities

outside boundary layers and in modes with very weak dissipation. SOMS uses the following method to reduce such numerical diffusion.

The diffusion coefficients are composed of a user-specified nominal contribution plus the contribution from the turbulence closure scheme (if used) plus a numerical contribution. This simple additive approach avoids logical decisions or maximum and minimum functions that vectorize slowly. The numerical contribution is directional. In each direction the numerical diffusive flux contribution is such that, in the absence of other diffusive contributions, the cell Reynolds number is equal to a user-specified cell Reynolds number. The directionality reduces the numerical diffusion effects and avoids unphysical oscillations.[17]

When the flow is parallel to grid lines, the numerical diffusion normal to the flow is zero. This is ideal, as gradients parallel to the flow are generally small compared to gradients normal to the flow.

At rigid boundaries, momentum fluxes normal to the boundary can be large, and can be specially treated as control volume sources, as described above in section 2.3.

2.6. *Coriolis and vertical diffusion terms*

The time scales of primary interest in ocean circulation models are long compared to the Coriolis time scale. SOMS resolves the Ekman-like bottom boundary layer, using a log-linear vertical co-ordinate, as described in detail in Appendix IV. Thus, flow features with sub-Coriolis diffusion time scales are resolved. To avoid undesirable time-step restrictions, both Coriolis and vertical diffusion terms are integrated implicitly in the boundary layer.

Originally, we used a time-splitting approach in which the Coriolis and vertical diffusion terms were integrated separately, with implicit numerical integration of the diffusion terms followed by analytic integration of the Coriolis terms. Although such a time-splitting approach was stable for time steps that were very large compared to time-step limits for explicit schemes, the results were very inaccurate and unphysical whenever these explicit stability limits were exceeded. However, we found that realistic results at large time steps are obtained by solving the control-volume space-integrated form of the following equations involving implicitly coupled Coriolis and vertical diffusion terms:

$$(u^{n+1} - u^n)/\Delta t = fv^N + (ku_z^N)_z + U,$$

$$(v^{n+1} - v^n)/\Delta t = -fu^N + (kv_z^N)_z + V,$$

where $(\ )^N = [(\ )^n + (\ )^{n+1}]/2$, f is the Coriolis parameter, k is the vertical diffusion coefficient and U and V are known (explicitly treated) terms.

These equations correspond to equations (4) given in section 3. This system was not accurately solved by our original time-splitting approach.

There appears to be a lesson here regarding implicit schemes in general. From our experience, it appears that, to avoid unrealistic results with implicit schemes, all terms *whose time scales are exceeded* must be accurately coupled. Fractional-step and time-split schemes, such as we originally tried, and related ADI schemes do not generally accomplish accurate coupling, even when the scheme is stable. This problem was also noted in a detailed analysis of a linearized fully implicit scheme.[18]

The SOMS implicit Coriolis–diffusion coupling requires solving two coupled equations which require special care. When the time step is larger than the explicit inertial (Coriolis) limit, ordinary relaxation fails. To circumvent this, SOMS solves the implicitly coupled Coriolis terms directly during each implicit iteration on the vertical diffusion terms, as follows (for constant k):

$$[u^{n+1}/\Delta t - fv^{n+1}/2 + ku^{n+1}/(\Delta z)^2]^m = U^{m-1},$$
$$[v^{n+1}/\Delta t + fu^{n+1}/2 + kv^{n+1}/(\Delta z)^2]^m = V^{m-1},$$

where U and V are known from previous inner iterations and time steps and m is the inner iteration index. One inner iteration per time step on the diffusion terms is stable and acceptably accurate with the time steps normally used.

In the above implicit Coriolis–diffusion treatment, the Coriolis terms conserve energy exactly (algebraically). Analogous treatment of spherical curvature terms (in which f is replaced by u/r, where u is the zonal velocity component and r is the distance to the global rotation axis) leads to exact energy conservation by these terms. The analogous swirl curvature terms that often dominate non-geophysical flows in cylindrical co-ordinates can also be treated with an analogous approach that conserves energy *exactly*.

2.7. *Filtered leap-frog–trapezoidal time integration*

In the SOMS time integration, each step is leap-frogged around the advanced time level of the previous step. In contrast to the classical leap-frog scheme, this is accomplished by averaging the old and new values at the end of each step, to create initial values (denoted by a tilde) for the next step:

$$(q^{n+1} - \tilde{q}^n)/\Delta t = Q(q^{n+1/2}),$$
$$\tilde{q}^{n+1/2} = (q^n + q^{n+1})/2,$$
$$(q^{n+3/2} - \tilde{q}^{n+1/2})/\Delta t = Q(q^{n+1}),$$
$$\vdots$$

where q is any predicted quantity and Q is the spatial operator in the dynamic equation.

This scheme was earlier used by Dietrich and Wormeck.[19] Its properties are analysed in Appendix V. It is conditionally stable for advection–diffusion equations and is not prone to time splitting, in contrast to the leap-frog scheme. (The leap-frog scheme is unconditionally unstable for diffusion terms.) This scheme strongly damps unphysical high time-frequency oscillations that can result from inaccurate initial conditions. It is first-order accurate in time, and artificially damps all temporal oscillations. However, it has identically zero second-order damping for truly steady solutions. Thus, although it artificially damps all temporal oscillations, the error is not severe for quasisteady small-scale boundary layer features and typical quasisteady ocean eddies with the time steps normally used in the present version of SOMS.

The present version of SOMS uses an explicit time integration scheme for internal gravity–inertia wave terms. Since such waves have time scales several orders of magnitude smaller than flow speeds (and also Rossby wave speeds for the dominant transient eddies), this limits the SOMS time step so that the Courant number is about 0·01. Thus, the time scales of modes that dominate the oceanic general circulation are well resolved and are only weakly damped. Internal waves are more strongly damped, but these are relatively small amplitude in the real ocean and interact very weakly with the oceanic general circulation, so there can be little loss of accuracy due to this damping.

In the future, we plan to modify SOMS so that much longer time steps can be taken (see section 5), which could lead to substantial damping of dominant oceanic general circulation time scales with the present filtered scheme. Such damping can be reduced by using a weighted combination of the present scheme with the leap-frog scheme, as described and analysed in Appendix V. Such a combined scheme can be stable for all terms, while having reduced damping compared to the present scheme. Although it appears to have similar properties to previous filtered schemes

such as described and analysed by Robert[20] and by Asselin,[21] these *appear* more complicated to analyse and apply. These schemes appear as post-processors to a general time integration scheme, whereas the present filtered scheme is a stand-alone time integration scheme that can be used in weighted combination with other time integration schemes.

In the present integration scheme, the advanced-time-level non-divergent velocity is centred for the next step and is used in all advection calculations. (Other advanced time level quantities also provide centred initial guesses for the next time step.) Thus, the convection terms are linear due to the known advection velocity in the middle of any time step. The resulting linear conservation equations could be solved implicitly to get an exact trapezoidal treatment with respect to the conserved quantities.

Although the present version of SOMS does not solve such an implicit system directly, SOMS conservation equations can optionally be iterated towards such an implicit trapezoidal approximation, if the time step is less than the explicit advection time-step limit. To exceed this limit and still obtain accurate results, one must solve the coupled two-dimensional implicit linear system accurately, as noted in section 2.6. This cannot be done with the present version of SOMS, owing to the lack of convergence of the optional iterations when the limit is exceeded. However, it can be done by resolving the flow into a base state plus deviations from the base state,[22,23] and using general elliptic solvers such as described by Dietrich[22,24] and by Roache[25] to solve linearized equations for the deviations.

We believe that such implicit treatment of convection terms would be useful in ocean circulation models, as the scheme would be second-order accurate in time, achieve exact quadratic conservation by convection terms, and avoid non-linear instability even with large Courant numbers.

2.8. *Turbulence closure*

SOMS uses the Mellor–Yamada level-2·5 turbulence closure scheme described by Mellor and Yamada[14] and used by Peggion[26] for the ocean bottom boundary layer. This scheme includes a transport equation for the turbulent eddy kinetic energy (E). The turbulent eddy length scale (L) is calculated from

$$L_0 = c \int_0^\infty zq \, dz \Big/ \int_0^\infty q \, dz,$$

$$L = kz/(kz/L_0 + 1),$$

where z is the distance from the bottom topography, c is an empirical constant and k is the Karman constant. This length scale is needed in a turbulence closure scheme that relates turbulent eddy energy to eddy diffusivity which is used in the mean flow equations. Bottom boundary conditions are based on a theoretical 'log law of the wall' (Appendix IV) also as described by Mellor and Yamada.[14]

3. THE DISCRETE CONTROL VOLUME EQUATIONS

In this section, we give the actual control volume equations solved by the FSM and TSM submodels given above. The corresponding continuum equations are in Appendix I. These submodels at present use the beta-plane approximation (in which the vertical component of

the earth's rotational angular velocity is assumed to vary linearly with latitude). Both submodels use a theoretically motivated stretched log-linear vertical co-ordinate to resolve boundary layers. Vertical derivative transformations are given in Appendix IV. The equations solved in the special case of a linear vertical co-ordinate are given below.

The control volume equations involve flux quantities, which involve time and space averages (to obtain the necessary interpolations). To concisely denote such averages, we use upper case superscripts, as follows:

$$F^{I,j,k,n} = (F^{i,j,k,n} + F^{i+1,j,k,n})/2, \text{ etc.} \tag{1}$$

where $F^{i,j,k,n} = F(i\,\Delta x, j\,\Delta y, k\,\Delta z, n\,\Delta t)$.

We also denote the advection velocity components by using the superscript 'A' in place of the time superscript (e.g. $u^{i,j,k,A}$, $v^{i,j,k,A}$, $w^{i,j,k,A}$). This non-divergent advection velocity was determined at the advanced time level of the previous time step, which is the middle of the present time step in our modified leap-frog time integration scheme described above. The advection velocity components are the same as the initial guesses for the time-averaged velocity components ($u^{i,j,k,N}$, $v^{i,j,k,N}$, $w^{i,j,k,N}$) that are optionally iterated within a time step.

Using the above notation, we now define quantities that are calculated and used in the energy, mass and momentum conservation equations, and in the turbulence closure equations. The Boussinesq approximation is used, in which density variations are addressed only in the hydrostatic relation, and depend only on temperature and salinity.

First, all fluxes are calculated, as follows:

$$\begin{aligned}
\underline{\mathrm{UU}}^{i,j,k} &= u^{I,j,k,A} u^{I,j,k,N} - \mathrm{CX}^{I,j,k}(u^{i+1,j,k,N} - u^{i,j,k,N})/\Delta x,\\
\underline{\mathrm{VV}}^{i,j,k} &= v^{i,J,k,A} v^{i,J,k,N} - \mathrm{CY}^{i,J,k}(v^{i,j+1,k,N} - v^{i,j,k,N})/\Delta y,\\
\underline{\mathrm{UV}}^{i,j,k} &= u^{i,J,k,A} v^{I,j,k,N} - \mathrm{CX}^{i,J,k}(v^{i+1,j,k,N} - v^{i,j,k,N})/\Delta x,\\
\underline{\mathrm{VU}}^{i,j,k} &= v^{i,J,k,A} u^{I,j,k,N} - \mathrm{CY}^{I,j,k}(u^{i,j+1,k,N} - u^{i,j,k,N})/\Delta y,\\
\underline{\mathrm{WU}}^{i,j,k} &= w^{I,j,k+1,A} u^{i,j,K,N} - \underline{\mathrm{KM}}^{I,j,k}(u^{i,j,k+1,N} - u^{i,j,k,N})/\Delta z,\\
\underline{\mathrm{WV}}^{i,j,k} &= w^{i,J,k+1,A} v^{i,j,K,N} - \underline{\mathrm{KM}}^{i,J,k}(v^{i,j,k+1,N} - v^{i,j,k,N})/\Delta z,\\
\underline{\mathrm{UT}}^{i,j,k} &= u^{i,j,k,A} T^{I,j,k,N} - \mathrm{CX}^{i,j,k}(T^{i+1,j,k,N} - T^{i,j,k,N})/\Delta x,\\
\underline{\mathrm{VT}}^{i,j,k} &= v^{i,j,k,A} T^{i,J,k,N} - \mathrm{CY}^{i,j,k}(T^{i,j+1,k,N} - T^{i,j,k,N})/\Delta y,\\
\underline{\mathrm{WT}}^{i,j,k} &= w^{i,j,k+1,A} T^{i,j,K,N} - \underline{\mathrm{KH}}^{i,j,k}(T^{i,j,k+1,N} - T^{i,j,k,N})/\Delta z.
\end{aligned} \tag{2}$$

CX and CY are horizontal diffusion coefficients, located at u and v positions, respectively, needed to avoid unphysical numerical oscillations.[17] $\underline{\mathrm{KM}}$ and $\underline{\mathrm{KH}}$ are eddy vertical momentum and heat transfer coefficients with contributions from the turbulence closure submodel. $\underline{\mathrm{KM}}$ and $\underline{\mathrm{KH}}$ are located at the w positions to facilitate exact conservation of energy in the mean-to-turbulence kinetic energy conversion terms. Other scalar transport equations (such as salinity) are treated like the heat transport equation.

Next, the momentum flux divergences and pressure gradient terms are calculated as follows:

$$\begin{aligned}
\underline{U}^{i,j,k} &= -(p^{i+1,j,N} - p^{i,j,N} + \underline{\mathrm{UU}}^{i,j} - \underline{\mathrm{UU}}^{i-1,j})/\Delta x - (\underline{\mathrm{VU}}^{i,j} - \underline{\mathrm{VU}}^{i,j-1})/\Delta y\\
&\quad + (\underline{\mathrm{WU}}^{i,j,k} - \underline{\mathrm{WU}}^{i,j,k-1})/\Delta z,\\
V^{i,j,k} &= -(p^{i,j+1,N} - p^{i,j,N} + \underline{\mathrm{VV}}^{i,j} - \underline{\mathrm{VV}}^{i,j-1})/\Delta y + (\underline{\mathrm{UV}}^{i,j} - \underline{\mathrm{UV}}^{i-1,j})/\Delta x
\end{aligned} \tag{3}$$

$$+(\underline{\mathrm{WV}}^{i,j,k}-\underline{\mathrm{WV}}^{i,j,k-1})/\Delta z.$$

The momentum conservation equations at scalar cell centres are as follows:

$$\begin{aligned}(u^{I,j,k,n+1}-u^{I,j,k,n})/\Delta t &= fv^{i+1,J,k,N}+U^{I,j,k}\\ (v^{i,J,k,n+1}-v^{i,J,k,n})/\Delta t &= -fu^{I,j+1,k,N}+V^{i,J,k}.\end{aligned}\tag{4}$$

The Coriolis terms in equations (4) conserve energy exactly. Replacing the Coriolis parameter f in equations (4) by $u^{i,j,k,\mathrm{A}}/r^j$ (see above) gives a similarly conservative equation for spherical and cylindrical curvature terms.

After solving equations (4) for the new horizontal velocity at the scalar cell centres, the velocity components are interpolated back to their original staggered positions. The vertical velocity is then calculated by vertical integration of the mass continuity equation from a specified zero top boundary condition. The result generally does not satisfy the bottom boundary condition, but the top pressure is corrected as described in Appendix II, and the horizontal and vertical velocity response to the pressure correction is calculated. The resulting vertical velocity satisfies its bottom condition exactly.

Although fully confident that the hydrostatic assumption is accurate for ocean circulation features to be addressed by SOMS, we have evaluated this approximation with a two-dimensional non-hydrostatic pressure calculation using the full Navier–Stokes equations. The difference in the results was found to be of the same order as the ratio of the vertical to horizontal scale of the flow, which is small for large-scale ocean circulation features to be directly addressed by SOMS.

Next, scalar transport equations are solved. All scalar-transport equations are similar to the following thermal transport equation:

$$\begin{aligned}(T^{i,j,k,n+1}-T^{i,j,k,n})/\Delta t = &-(\underline{\mathrm{UT}}^{i,j,k}-\underline{\mathrm{UT}}^{i-1,j,k})/\Delta x\\ &-(\underline{\mathrm{VT}}^{i,j,k}-\underline{\mathrm{VT}}^{i,j-1,k})/\Delta y-(\underline{\mathrm{WT}}^{i,j,k}-\underline{\mathrm{WT}}^{i,j,k-1})/\Delta z\end{aligned}\tag{5}$$

The conservation equations can optionally be iterated by returning to equations (2). Finally, hydrostatic pressure is calculated from the advanced time level temperature to provide a centred first guess for the next time step, and all fields are averaged to the intermediate time level to provide initial values for the next time step.

This completes the updating of the mean flow quantities. The turbulence quantities are updated as follows. The fluxes of turbulence kinetic energy density (C) are calculated from

$$\begin{aligned}\underline{\mathrm{UE}}^{i,j,k} &= u^{i,j,K,\mathrm{A}}E^{I,j,k,N}-\mathrm{CX}^{i,j,K}(E^{i+1,j,k,N}-E^{i,j,k,N})/\Delta x,\\ \underline{\mathrm{VE}}^{i,j,k} &= v^{i,j,K,\mathrm{A}}E^{i,J,k,N}-\mathrm{CY}^{i,j,K}(E^{i,j+1,k,N}-E^{i,j,k,N})/\Delta y,\\ \underline{\mathrm{WE}}^{i,j,k} &= w^{i,j,K,\mathrm{A}}E^{i,j,K,N}-\underline{\mathrm{KE}}^{i,j,K}(E^{i,j,k+1,N}-E^{i,j,k,N})/\Delta z.\end{aligned}\tag{6}$$

$\underline{\mathrm{KE}}$ is a turbulent diffusion coefficient, defined by

$$\underline{\mathrm{KE}}=qLS_{\mathrm{q}}$$

where $q=(2E)^{1/2}$, L is the eddy length scale, determined as described in section 2.8, and S_{q} is an empirical constant ($S_{\mathrm{q}}=0{\cdot}2$; see Reference 14).

These fluxes are used to update E from

$$\begin{aligned}(E^{i,j,k,n+1}-E^{i,j,k,n})/\Delta t = &-(\underline{\mathrm{UE}}^{i,j,k}-\underline{\mathrm{UE}}^{i-1,j,k})/\Delta x-(\underline{\mathrm{VE}}^{i,j,k}-\underline{\mathrm{VE}}^{i,j-1,k})/\Delta y\\ &-(\underline{\mathrm{WE}}^{i,j,k}-\underline{\mathrm{WE}}^{i,j,k-1})/\Delta z+\underline{\mathrm{KM}}^{i,j,k}\{[(u^{I-1,j,k+1,n}-u^{I-1,j,k,n})/\Delta z]^2\\ &+[(v^{i,J-1,k+1,n}-v^{i,J-1,k,n})/\Delta z]^2\}\end{aligned}$$

$$-\alpha q(T^{i,j,k+1,n} - T^{i,j,k,n})/\Delta z - q^3/B, L, \quad (7)$$

where B_1 is an empirical constant ($B_1 = 16{\cdot}6$; see Reference 14) and α is the thermal expansion coefficient for water. Note that only temperature effects on the density field are included. Salinity effects were not considered in these preliminary studies, but certainly will be added later.

B and L are then used to determine the eddy diffusivity from the Mellor–Yamada turbulence closure scheme. The terms representing conversion of mean flow kinetic energy to turbulence kinetic energy conserve total mean flow plus turbulence kinetic energy algebraically.

In both the free-stream and thin-shell submodels, turbulence dissipation terms are solved implicitly, with a first-order backward time difference scheme to give more realistic behaviour and to avoid possible unphysical negative E when the time step is large (compared to the dissipation time scale).

4. SOMS APPLICATION TO AN IDEALIZED NORTH ATLANTIC OCEAN

For better comparison with other primitive equation codes such as those of Bryan[5] and Semtner,[6] we created a simplified general circulation model version of SOMS, by eliminating the thin-shell submodel and the Mellor–Yamada level-2·5 turbulence closure scheme. In this section, we use this version to demonstrate the numerical performance of SOMS. More detailed results and physical interpretations are given by Dietrich and Marietta.[12] The fully turbulent version will be evaluated in a separate paper on boundary layer results.

In Table I, the numerical performance of SOMS is compared with that of the Bryan–Semtner model. In the 200 km runs, all input parameters for SOMS except time-step size correspond to those used for the Bryan–Semtner model.

The Bryan–Semtner model calculation actually used a long (twelve hour) time step for the internal energy and salinity conservation equations, and a short (half hour) time step for the momentum conservation equations. This corresponds to the time-step ratio given in example cases in the model documentation, and is about half the empirically determined stability limit for that ratio.

Only one short time step is calculated for the momentum equations for each long time step in the temperature and salinity equations. This time-step mismatch is suggested in the model

Table I. Model comparison. CPU times are for a Cray 1 computer

Model	Resolution	Horizontal grid interval	dt	CPU per step	CPU per day
Actual run parameters					
Bryan–Semtner	23 × 18 × 6	200 km	147 min	0·048 s	0·470 s
SOMS	23 × 18 × 6	200 km	720 min	0·022 s	0·044 s
SOMS	60 × 48 × 6	75 km	240 min	0·104 s	0·625 s
Estimated run parameters					
Bryan–Semtner	60 × 48 × 6	75 km	55 min	0·227 s	5·94 s

With 200 km resolution, the Bryan–Semtner calculation actually used a 30 minute time step for the momentum conservation equations and a 720 minute time-step for the thermal energy and salinity conservation equations. This time-step combination is about half the longest empirically stable combination possible under the condition that the ratio of the thermal energy equation time step to the momentum equation time-step is 24, as in the examples in the Bryan–Semtner model documentation. For appropriate comparison with SOMS, the value given in the table is the square root of the product of the long and short time-step sizes, and is about half the empirical time-step stability limit that would result if the time-steps were equal.

documentation to reduce the calculation required to approach a steady state. The motivation for this is addressed by Semtner.[27]

For appropriate comparison to SOMS numerical performance, the time step given in Table I for the Bryan–Semtner model calculation is defined as the square root of the product of the long and short time steps, and is about half the empirical limit that would result if the time steps were equal.

The general circulation version of SOMS has also been applied to higher resolution (75 km) studies, as described by Dietrich and Marietta.[12] SOMS performance in these studies is also given in Table I. Similar calculations were attempted with the Bryan–Semtner model but discontinued due to its large computing cost (see the estimate in Table I) and required numerical diffusion (see below).

The Bryan–Semtner model must resolve the *model* Munk layer to avoid unphysical numerical oscillations.[28] The Munk layer scale is determined by scaling the vertical vorticity component transport equation, assuming a balance between the horizontal diffusion of relative vorticity and the advection of the vertical component of earth's vorticity. Such balance prevails near ocean basin boundaries. This means that unrealistically large horizontal diffusion must be used unless the true *oceanic* Munk layer is resolved. In the 200 km resolution case in Table I, both models used a horizontal eddy momentum transfer coefficient of $10^9\,cm^2/s$. This large eddy viscosity ostensibly represents subgrid-scale eddy-diffusion effects, but is at least an order-of-magnitude larger than plausible. This is required by the Bryan–Semtner model owing to its Munk layer constraint. The two models given similar results in this high viscosity case where both models are applicable and can be compared. However, the SOMS vertical velocity is less noisy. Further, SOMS is applicable to realistic horizontal diffusion cases that are not addressable by the Bryan–Semtner model unless much greater resolution is used. For example, with 200 km resolution, SOMS gives a reasonable vertical velocity field using a horizontal diffusivity of $10^7\,cm^2/s$, whereas the vertical velocity field from the Bryan–Semtner model is quite noisy even with $10^9\,cm^2/s$ diffusivity.

5. FUTURE WORK

To further improve SOMS performance and accuracy, a number of features can be added in the future. Some of these are described here.

5.1. Implementation of curvilinear co-ordinate systems

As noted in section 2.2, the SOMS thin-shell boundary layer submodel ignores boundary curvature effects, which is a commonly used boundary layer approximation. To address such curvature effects, an appropriate curvilinear co-ordinate system must be added to SOMS. To address the curvature effects on subgrid-scale turbulence, the turbulence closure scheme must also be modified, as noted in section 5.2.

5.2. Improvement of the turbulence closure scheme

The Mellor–Yamada level-2·5 turbulence closure scheme, and related popular schemes based on transport of turbulence scalar quantities, have several problems that should be addressed.

The determination of turbulence length scale by the Mellor–Yamada level-2·5 turbulence closure scheme used by SOMS (see section 2.8), although reasonable, is not based on fundamental fluid conservation laws and is known to be problematic. A possible alternative

length scale determination involves using an equation for the mean squared eddy vector vorticity (SEV). A transport equation for SEV can be derived in an analogous manner to the one for turbulence kinetic energy (E). The SEV equation would have source and sink terms related to corresponding terms in the E equation (through the square of the turbulence length scale, L^2). Also, L would be related to $(E/\mathrm{SEV})^{0.5}$ in the turbulence closure relations. This determination is based on application of the conservation equations for both turbulence kinetic energy and length scale determination, and thus might lead to more realistic and universally applicable turbulence closure models.

The turbulence kinetic energy source term used by the Mellor–Yamada level-2·5 scheme is designed to address shear flows with buoyancy effects, but does not address the effect of large fluid acceleration forces associated with curved flow trajectories. Such curved flow can affect turbulence kinetic energy generation, especially along curved boundaries, according to Taylor (centrifugal) instability theory, and can dominate over shear and buoyancy effects addressed by the Mellor–Yamada level-2·5 scheme. Such flow curvature effects depend on details of the flow distribution. Such effects can be very complicated, as is easily seen by the vast literature on experimental flows in the classical Taylor–Couette configuration, and might require direct prediction of Reynolds stresses.

5.3. Avoidance of the internal wave time-step limit

The rigid-lid boundary condition used in the SOMS pressure calculation, as described in Appendix II, eliminates the highest frequency surface wave components. However, high-frequency internal waves can still undesirably limit the time step compared to quasigeostrophic models. Instead of calculating pressure as described above, several methods can be used to remove this time-step restriction. One is to physically remove the internal waves by using a balance equation (as described below). Another procedure is to integrate the internal wave terms implicitly, along with the Coriolis term and, possibly, the vertical diffusion terms in boundary layers. Work on this latter procedure has begun.

To remove internal waves from the calculation, a steady-state approximation to the horizontal divergence of the momentum conservation equation is used to derive a relation that diagnostically determines vertical velocity. The geostrophic relation (between the vertical vorticity component and the Laplacian of the pressure gradient) is an approximation to this balanced equation. A balanced vertical velocity equation (derived from this steady-state approximation to the horizontal divergence equation, together with the vertical vorticity component equation, the thermal heat transport equation and the incompressibility relation) can include terms ignored by quasi-geostrophic models and is analogous to the 'omega' equation often used diagnostically to determine atmospheric vertical velocity.[29] Using it to determine vertical velocity physically eliminates high-frequency internal modes, while leaving vertical velocity relatively unconstrained in the dominant quasibalanced geophysical flow components of primary interest. (This does not include tidal components or internal waves. However, such oceanic flow components are less important in the ocean general circulation than internal waves in the atmosphere due to coupling of large-scale atmospheric vertical motions to latent-heat release, especially in strong energy converting events such as east coast winter storms, as noted by Dietrich and Brunet.[30])

The key to the elimination of the high-frequency internal waves is to ignore the local time derivative term in the horizontal divergence equation. A possible refinement would be to include a time-filtered form. Use of a sample running lagged time filter would require storage of only one extra field.

The oceanic 'omega' equation would be a three-dimensional elliptic equation. Non-elliptic

regions of negative static stability should be weakly non-elliptic and treatable by explicitly marching the full equations. It would probably not require much iteration to stabilize the computation for time steps large compared to the explicit internal wave limit. After using the oceanic 'omega' equation to determine the oceanic vertical velocity field, the pressure field would be adjusted at one level to provide the appropriate horizontal velocity divergence to balance the divergence of the vertical velocity field, the hydrostatic relation would determine pressure at the remaining levels and horizontal velocity could then also be adjusted at all levels. If the calculation is internally consistent, the three-dimensional velocity would then be non-divergent.

5.4. *Reduction of numerical diffusion*

The directed diffusion coefficients is SOMS are ideal when the flow is parallel to grid lines (section 2.5). However, when the flow is not parallel to grid lines, cross-flow numerical diffusion occurs with the present approach. Such cross-flow numerical diffusion can be reduced as follows.

The numerical diffusion at a given grid point (control volume centre) can be calculated using a diffusion operator approximated from field values at three points along a line parallel to the flow and through the given point. One of the three field values is the value at the given point. The other two required field values can be calculated by interpolation from nearby points. The reduced dissipation resulting from replacing the present simpler approach in SOMS by this numerical diffusion calculation should more than compensate for any conservation errors introduced.

Generally, numerical diffusion is much stronger than physical diffusion across water mass boundaries (such as the Mediterranean, Antarctic and Arctic waters). Such unphysical numerical diffusion can be reduced by using a multi-phase flow formulation with reduced diffusion across phase boundary surfaces.[19] For example, the water masses could all be separate phases, with appropriately small interphase diffusion.

5.5. *Inclusion of non-hydrostatic effects*

The use of the hydrostatic approximation in SOMS (Appendix II) might not be appropriate for some boundary-layer processes, especially when the topography is steep and when small horizontal scales are involved in boundary layer separation. A possible refinement of SOMS that includes non-hydrostatic effects while avoiding solving a three-dimensional elliptic equation for pressure, and works at least for weakly non-hydrostatic flow, is given in Appendix II.

5.6. *Implementation of direct implicit solvers*

Direct solvers could be used instead of the iterative approach used by SOMS to solve the implicitly coupled Coriolis and vertical diffusion terms (section 2.7). However, direct solvers can encounter difficulty outside the boundary layer region, where the diffusion coefficients are nearly zero. This difficulty can be avoided by using the direct solver only in the boundary layer, where the diffusion coefficients are large enough to restrict the time step for explicit schemes.

6. SUMMARY AND CONCLUDING REMARKS

The Sandia ocean modelling system (SOMS) is a system of primitive equation numerical models.

The master version is three dimensional, and divides the modelled ocean into lower and upper subdomains. The lower subdomain is addressed by a thin-shell bottom boundary layer submodel, and the upper by a free-stream submodel. The lower subdomain is a thin layer of constant thickness that includes the bottom mixed layer, and the upper subdomain is the overlying ocean. This coupled system facilitates efficient modelling of the bottom boundary layer with realistic topography. Coupling is accomplished through continuity conditions applied at the common interface, which is an undulating surface at the top of the thin-shell submodel domain. The two submodels can also be run separately, or coupled to other appropriate models. The free-stream submodel can address the free stream flow (with bottom topography) and/or the top boundary layer. To efficiently and accurately address boundary layer dynamics, both submodels use a stretched vertical co-ordinate normal to the ocean boundary, and both have an optional Mellor–Yamada level-2·5 turbulence closure scheme with associated subgrid scale turbulence energy and length scale predictive relations. Currently, the thin-shell submodel ignores co-ordinate curvature effects associated with bottom topography, a common boundary layer approximation.

Briefly, the numerical features of SOMS also include a staggered (Arakawa 'c' grid) control volume approach, boundary fluxes modelled by control volume sources, each diffusion coefficient being a vector with a numerical contribution parallel to the local velocity and determined by a user-specified cell Reynolds number limit, iterative implicit solution of coupled Coriolis and vertical diffusion terms, and of turbulence dissipation and diffusion, modified leap-frog time integration, exact (algebraic) mass, energy, momentum and species conservation by finite-difference approximation to convective transport terms, and by the exchange between mean flow kinetic energy and subgrid scale turbulence kinetic energy, and rigid-top pressure directly determined from vertically integrated conservation equations.

Each submodel separately reproduces previously published results, but does so with notable numerical advantages (i.e. speed and economy). Moreover, SOMS is able to produce what appear to be reasonable results in situations in which older models break down. Reliable, efficient models for detailed comparison are not readily available. However, SOMS and the Bryan–Semtner code produce similar results in problems to which both are applicable. Unlike the Bryan–Semtner code, SOMS is not constrained to resolve the model Munk layer; and, for a given resolution, SOMS is much faster on a Cray-I computer.

The good performance of SOMS with low dissipation and large time step is primarily due to numerical features described in section 2. The number of computations per time step is also reduced by determining surface pressure directly by the conservation equations (Appendix II) rather than introducing a barotropic stream function, by the omission of spherical curvature terms in the present version of SOMS, by the combining of SOMS advective and diffusive fluxes before taking differences, by the omission of the salt conservation equation, including only temperature and density in the equation of state, and by using central memory to store often-used arrays and thereby reduce data handling.

ACKNOWLEDGEMENTS

We warmly acknowledge the extensive contributions and physical guidance of Dr. Georges Weatherly throughout this model development. We thank Dr. Harley Hurlburt and Dr. William Simmons for valuable comments and advice in developing SOMS and on this manuscript. This research was supported by Sandia National Laboratories under Contract DE-AC04-76DP00789 for the United States Department of Energy.

APPENDIX I: SOMS CONTINUUM EQUATIONS

The following continuum equations correspond to the SOMS control volume equations given in section 3 and use similar notation:

$$u_t = -p_x + fv - \nabla\cdot(u\mathbf{V}) + (\mathrm{CX}\,u_x)_x + (\mathrm{CY}\,u_y)_y + (\mathrm{KM}\,u_z)_z,$$

$$v_t = -p_y - fu - \nabla\cdot(v\mathbf{V}) + (\mathrm{CX}\,v_x)_x + (\mathrm{CY}\,v_y)_y + (\mathrm{KM}\,v_z)_z,$$

$$p_z = \varepsilon T g,$$

$$T_t = -\nabla\cdot(T\mathbf{V}) + (\mathrm{CX}\,T_x)_x + (\mathrm{CY}\,T_y)_y + (\mathrm{KH}\,T_z)_z,$$

$$E_t = -\nabla\cdot(E\mathbf{V}) + (\mathrm{CX}\,E_x)_x + (\mathrm{CY}\,E_y)_y + (\mathrm{KE}\,E_z)_z + \mathrm{KM}(u_z^2 + v_z^2) - \alpha g T_z - q^3/B_1 L.$$

APPENDIX II: PRESSURE DETERMINATION IN SOMS

SOMS uses the hydrostatic approximation. Thus, if the pressure is known at one level, its value everywhere else is determined from the density field, using the hydrostatic relation. Starting with a guessed (or most recently calculated) pressure at one level (say the surface), the hydrostatic relation is integrated to obtain pressure everywhere below. The resulting pressure is then substituted into the momentum conservation equations, and a new horizontal velocity is calculated based on the trial surface pressure. Vertical velocity, again based on this trial surface pressure, is then calculated by integrating the mass continuity downward from the top surface (where vertical velocity is zero due to the rigid-lid approximation used by SOMS). The resulting vertical velocity satisfies its bottom boundary condition (zero, or a prescribed value from a boundary-layer submodel) if and only if the vertically integrated horizontal divergence is correct. It follows that the error in the bottom boundary condition is related to the error in the guessed surface pressure (at $z = 0$), $\delta p_S(x, y)$:

$$\nabla^2 \delta p_S(x, y) = \tilde{w}_B(x, y)/(D\,\Delta t),$$

where $\delta p_S(x, y) = p(x, y, 0) - \tilde{p}_S(x, y)$, D is the ocean depth and $\tilde{w}_S(x, y)$ is the bottom vertical velocity resulting from the original (guessed) $\tilde{p}_S(x, y)$.

This two-dimensional Poisson relation, together with its appropriate Neumann (normal gradient) boundary conditions, can be derived directly from the vertically integrated control volume mass and momentum conservation equations. After solving this equation for δp_S, the result is added to $\tilde{p}_S$. The response of the horizontal velocity to δp_S is independent of depth, and is simply added to the original calculation. Vertical velocity can then be similarly adjusted by adding the appropriate depth-independent vertical divergence correction. The result satisfies both the bottom and top boundary conditions on vertical velocity. The procedure also satisfies the conservation equations (with the hydrostatic approximation representing the vertical momentum conservation equation) with the adjusted pressure.

The above procedure determines the flow uniquely from the conservation equations under the hydrostatic approximation. It also avoids conceptual and computational complications associated with using a stream function for the barotropic mode, especially when there are islands. However, it should be noted that since the proper boundary conditions for the surface pressure are Neumann (gradient), they must be consistent with the prescribed Poisson equation source term. This is automatically satisfied if both the Poisson difference equation for δp_S and its boundary conditions are derived from the control volume mass and momentum conservation equations, and there is no net mass flux through the modelled region boundaries (as required for incompressible flow in general). Of course, there is an arbitrary constant in the error pressure

field, which can conveniently be accounted for by assigning a boundary value to zero.

We have found that mild non-hydrostatic pressure effects can be included by a slight modification of this procedure. This is done by including acceleration terms when integrating the vertical momentum conservation equation to obtain pressure below the surface. When the ratio of the horizontal to vertical grid interval is large (of order two or more) everywhere, iterations on the vertical acceleration terms converge, and the scheme is stable. It thus yields results close to those using the more general pressure calculation procedure for incompressible flow.

APPENDIX III: MODEL COUPLING AND BOUNDARY CONDITIONS

The free-stream (FSM) and thin-shell (TSM) submodels of SOMS are coupled by continuity conditions imposed at their interface. The FSM influences the TSM only by its bottom pressure and temperature, which serve as upper boundary conditions for the TSM. The TSM influences the FSM only by its prediction of vertical convective fluxes at their interface.

Except for vertical velocity, TSM-FSM interfacial fluxes are numerically treated as sources in the lowest control volume equations (see section 2.3) of the FSM, whose boundary face or faces are numerically treated as closed (with no mean or turbulent transfers). The TSM determines these fluxes at its top boundary, which is parallel to the bottom topography. Interfacial fluxes involving turbulent and laminar viscosities are assumed to be negligible. This could be modified by including eddy transfers predicted by the TSM at its top, but these are very small if the bottom boundary layer is contained within the TSM domain. Although the TSM has no explicit topography, it is influenced by topography through its coupling to the FSM.

Wind stress and temperature or heat flux are specified at the top of the FSM. Again, these are numerically treated as specified sources of momentum and heat, with numerical boundary conditions of zero flux.

APPENDIX IV: STRETCHED LOG-LINEAR VERTICAL CO-ORDINATE

In order to model accurately thin log-profile boundary layers, a vertically stretched (log-linear) vertical co-ordinate is used near the ocean top (in the SOMS free-stream submodel) and ocean bottom (in the SOMS thin-shell submodel). The control volumes are then uniformly spaced in the stretched co-ordinate. Vertical derivatives used in flux calculations can then be accurately estimated (assuming that the fields are smooth in the stretched system) at the non-uniformly spaced (in z) control volume boundaries.

The stretched vertical co-ordinate, S, is defined by

$$S(z) = c_1 z + c_2 L(z), \tag{8}$$

where $L(z) = \ln(z/z_0)$, z_0 is a surface roughness parameter, c_1 and c_2 are defined such that $S(H) = H$ and $S(h) = nH/N$, H is the submodel total depth, h is the expected mixed layer thickness ($h < H$), N is the number of layers in the submodel and n is the number of layers between $z = 0$ and $z = h (n < N)$.

The layers are defined to be horizontal slabs bounded by horizontal planes at $S = (n-1)H/N$, $n = 1, 2, \ldots, N+1$. These planes form the top and bottom boundaries of the scalar control volume cells (for p, T, etc.) and for the horizontally staggered u- and v- control volume cells. Each scalar cell is considered to be wholly within or wholly outside of the water column, according to a user-specified flag array. The vertically staggered planes where $S = (n-1/2)H/N$, $n = 1, 2, \ldots, N$ form the top and bottom boundaries for turbulence kinetic energy (E) control volumes. Vertical velocity is defined at the top and bottom of the scalar cells, and is calculated

by integrating the incompressibility relation, starting with $w = 0$ at $S = 0$ (the ocean boundary in both submodels). Its value at $z = H$ in the thin-shell submodel is used as a bottom boundary condition for the free-stream submodel.

The two conditions for c_1 and c_2 are

$$H = c_1 H + c_2 L(H) \quad \text{and} \quad nH/n = c_1 h + c_2 L(h). \tag{9}$$

The solution to equations (9) is

$$c_1 = H[L(h) - (n/N)L(H)]/D \quad \text{and} \quad c_2 = H[(nH/N) - h]/D, \tag{10}$$

where $D = HL(h) - hL(H)$.

After calculating c_1 and c_2 from equations (10), z must be determined at all S grid positions ($nH/(2N)$, $n = 1, 2, \ldots, 2N - 1$). These values for z are needed to evaluate vertical derivatives that are used in flux calculations at discrete S levels (which are control volume boundaries):

$$\mathrm{d}(\ )/\mathrm{d}z = \mathrm{d}S/\mathrm{d}z\, \mathrm{d}(\ )/\mathrm{d}S = (c_1 + c_2/z)\, \mathrm{d}(\ )/\mathrm{d}S. \tag{11}$$

This determination can be made by using a Newton–Raphson iteration on z. The $\mathrm{d}(\ )/\mathrm{d}S$ operator is approximated using centred differencing on the uniform S grid. Similarly, centred interpolations are used when needed on the uniform S grid. The resulting approximations have second-order accuracy in S.[31] Thus, if the co-ordinate transformation is appropriate (i.e. the boundary layer profiles are smooth in S), accurate derivative approximations result. After the flux calculations, the control volume approach described in section 2 is applied to the control volumes separated by the non-uniformly spaced (in z) S surfaces.

The following theoretically motivated log-profile relation can be used to reduce the resolution required to model turbulent eddy interaction with mean boundary layer flow:

$$U(z) = (U_*/K) \ln(z/z_0), \tag{12}$$

where $U_* = q/(B_1)^{1/3}$.

Equation (12) can be used to determine the lowest level mean horizontal velocity (used as a boundary condition in the mean flow equations) from the low-level turbulence kinetic energy. This procedure, when applied to multidimensional flow, can produce unphysical horizontal velocity discontinuities near stagnation points, specifically when the turbulence kinetic energy is not small near such centres. Horizontal advection and diffusion can transport turbulence kinetic energy into such stagnation regions. (These are not considered in the log-layer theory based on locally deterministic boundary layers.) Also, vertical shears of the mean flow can exist even where the mean flow vanishes. This would give a source for turbulence kinetic energy. Although such discontinuity-producing effects should generally be small near stagnation points, caution should be taken in applying the log-layer method to multi-dimensional boundary layer models.

To clarify the use of equation (12), Figure 3 illustrates the staggered variables.

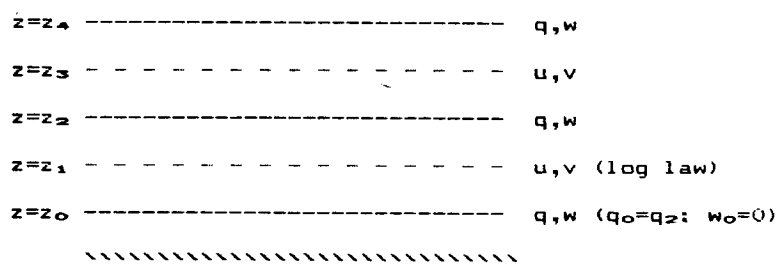

Figure 3. Schematic diagram showing vertically staggered variables and boundary conditions applied near ocean bottom

1. Mean flow quantities are determined at levels z_2 and above by using mean flow equations.
2. q and the turbulence length scale are determined at levels z_2 and above by using turbulence equations.
3. The turbulence length scale at level $z = z_0$ is assumed equal to the roughness scale multiplied by Von Karman's constant.
4. The mean velocity magnitude at level z_1 is determined from q_2 using equation (12) (noting that q is approximately independent of z in the lowest layer).
5. The mean velocity direction at level z_1 is assumed to be the same as that already known at level z_3. This determines the lowest level boundary conditions for the next iteration of the mean flow equations.

APPENDIX V: EVALUATION OF THE FILTERED LEAP-FROG–TRAPEZOIDAL TIME INTEGRATION METHOD

This Appendix presents a brief summary of the results in Reference 32, in which the filtered leap-frog–trapezoidal (FLT) scheme is analysed for the one-dimensional constant coefficient advection equation, and is shown to have some advantages for quasisteady flows. A modification (FLTW) using a weighted combination of FLT and leap-frog is developed which retains the advantages for steady flows and increases accuracy for time-dependent flows, and involves little coding effort.

We can define the FLT method economically, considering only the model one-dimensional advection equation,

$$q_t = -uq_x, \tag{13}$$

where u is the constant advection velocity. Adopting a concise notation, in which omitted superscripts and subscripts are understood to represent n and i, the leap-frog method is

$$q^{n+1} = q^{n-1} - c(q_{i+1} - q_{i-1}), \tag{14}$$

where $c = u\,\Delta t/\Delta x$ is the Courant number. The FLT method applies a time filter to (14), replacing q^{n-1} by

$$q^{n-1} = (1/2)(q^n + q^{n-2}). \tag{15}$$

A simple extension of the method involves a user-selected weighted combination of FLT with leap-frog, giving FLTW:

$$q^{n+1} = (w/2)(q^n + q^{n-2}) + (1-w)q^{n-1} - c(q_{i+1} - q_{i-1}). \tag{16}$$

FLTW reduces to FLT for $w = 1$, and to leap-frog for $w = 0$.

The operation count is evaluated including an additional multiplication for each local evaluation of Courant number c from local velocity u. In one-dimension, the penalties of FLT and FLTW compared to leap-frog are 50 and 100 per cent, respectively; these become 25 and 50 per cent in two-dimensions and 17 and 33 per cent in three-dimensions. Note that in a practical fluid dynamics code, these relative penalties would be reduced by the operations for viscous terms, pressure solutions, etc. The net penalty is considered small.

FLTW may be written in terms of an addition to leap-frog; rearrangement of (16) to fit the form of (14) gives

$$q^{n+1} = q^{n-1} - c(q_{i+1} - q_{i-1}) + (w/2)(q^n - 2q^{n-1} + q^{n-2}). \tag{17}$$

This form indicates clearly that the method has no spatial damping compared to the leap-frog method, but adds a time-only damping term; in a steady state, the added term is identically zero.

Neither leap-frog nor FLTW is self-starting, since another method must be used to initiate the multiple time levels. Neither moves the short wavelength (Λ) component of the solution; i.e. the $\Lambda = 2\,\Delta x$ component is stationary, except for (non-physical) boundary condition effects.[17] FLTW does not maintain a desirable property shared by most conventional methods; it does not preserve the exact solution for the special case of unity Courant number.

The (local) truncation error analysis of FLTW is performed using the standard Taylor series approach, giving

$$q_t = -uq_x + (w\Delta t/4)u^2 q_{xx} + O(\Delta x^2, \Delta t^2). \tag{18}$$

Although the smoothing operation (15) may appear to 'centre' the replacement for q^{n-1}, the resulting method is shown to be formally only first-order accurate in time. (Note that, in SOMS, the turbulent dissipation terms are also $O(\Delta t)$.) Interpreting (18) by the now-standard methods of heuristic stability analysis, FLTW represents the original continuum inviscid equation (13) to $O(\Delta t, \Delta x^2)$, but to $O(\Delta x^2, \Delta t^2)$ represents a viscous equation (with an effective Reynolds number of $4/w\,\Delta t$.) The positivity of this diffusion coefficient indicates at least conditional stability.

The von Neumann analysis of FLTW is somewhat involved because the method involves four time levels, and the complex eigenvalues are obtained from a cubic equation; details may be found in Reference 32. The analysis indicates a stability limit on the Courant number c of

$$c \leqslant 1 - w/2. \tag{19}$$

For the FLT method with $w = 1$, this gives a limit of $c \leqslant 1/2$. This limit has been verified experimentally. (Note that the time filtering of Asselin,[21] although more difficult to apply, gives a somewhat less restrictive limit of $c \leqslant 0{\cdot}57$.) For $w = 0$, the present FLTW method reverts to leap-frog with the usual restriction of $c \leqslant 1$.

The phase error behaviour has been evaluated experimentally by comparisons with the exact solution for an advected sine wave. Damping errors are indicated by the reduced peak amplitude, and horizontal shifts are the result of accumulated phase errors.

These tests show the results for situations relevant to time-dependent flows. The application of the FLTW method in the SOMS codes is perhaps closer to the other extreme of steady flows. In the true steady-flow situation, FLTW gives the same answers as any time differencing method which uses three-point centered space differencing (and is stable and does not decouple). However, the motivation for the FLTW modification to the leap-frog method is that leap-frog has a tendency to produce decoupled solutions at alternate time steps. This could be prevented by weighting leap-frog with any number of methods which do not themselves decouple: with FLT as in the present FLTW method, with upwind differencing, with Lax–Wendroff methods, etc.[17] However, the (two-point) upwind method produces a strong artificial viscosity effect in both transient and steady-state results, as is well known. The Lax–Wendroff method is not so easily adapted to turbulence terms; also, the mixed space–time formulation results in a peculiar property of the steady-state solutions being a weak function of the time step used, and it may be interpreted as displaying a steady-state artificial viscosity. (See Appendix B of Reference 17.) Thus, any comparisons which indicate roughly comparable performance for FLTW on a strongly transient problem may be regarded as a good evaluation of FLTW for quasisteady problems.

Figure 4 shows the results of the FLT method (FLTW with $w = 1$) applied to an initial sine wave with the limiting time step, $c = 1/2$, after one cycle. The amplitude is reduced to 0·548. It is clear that this performance is inadequate for transient problems. The FLT method may still be useful for steady-state problems, since the high temporal damping would reduce the computer CPU time required to attain a steady state. However, for strongly transient problems, it is clear that $w < 1$ is advisable.

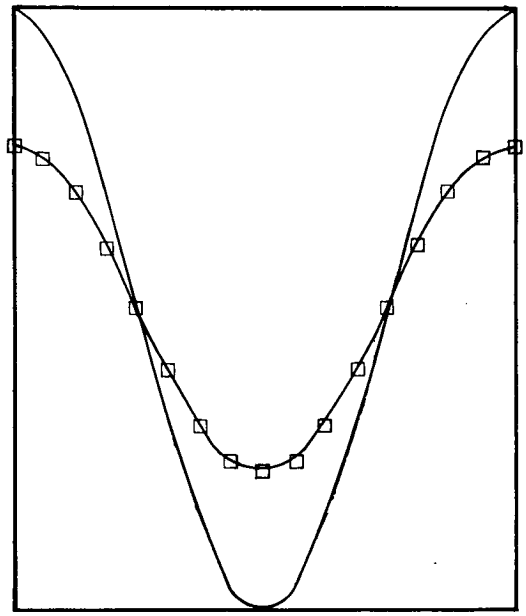

Figure 4. Exact solution and numerical solution (□) produced for $c = 1/2$ by the FLT method (FLTW with $w = 1$) after one cycle

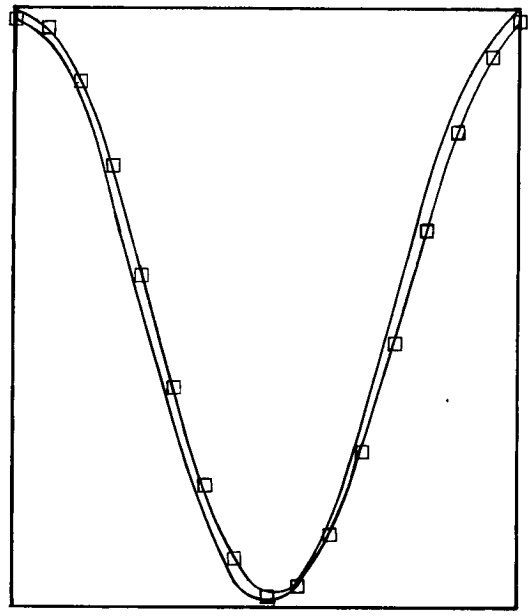

Figure 5. Exact solution and numerical solution (□) produced for $c = 1/2$ by the FLTW method with $w = 1/10$ after one cycle

Figure 5 shows the results of the FLTW method at $c = 1/2$ with $w = 1/10$, which is expected to be sufficient to prevent solution decoupling of the leap-frog method in steady-state problems. It

performs respectably well; the amplitude after one cycle is reduced to 0·967, certainly better than pure upwinding (0·537) and comparable to Lax–Wendroff (0·976) and leap-frog (0·994). Note that this experimental amplitude decrease is not the same as that which arises from the von Neumann analysis, which predicts zero damping (unity amplification factor) for leap-frog.[17]

Thus, the FLTW method applied to the model one-dimensional advection equation has been shown to be $O(\Delta t, \Delta x^2)$ accurate, and conditionally stable for Courant number $c \leqslant 1/2$. Unlike most methods, it does not preserve the exact solution for $c = 1$ or for its limit Courant number. Its artificial damping is purely temporal, possessing no artificial viscosity for steady-state problems. Designed to overcome the problem of solution decoupling exhibited by the leap-frog method, it involves at most a 33 per cent operation count penalty in three-dimensions compared to leap-frog (less for the full fluid dynamics equations). For strongly transient problems, the FLTW method with weighting parameter $w = 1/10$ or less performs reasonably well compared to leap-frog and Lax–Wendroff methods, as judged by damping error and accumulated phase error.

REFERENCES

1. M. G. Marietta and A. R. Robinson, 'Status and outlook of ocean modeling research: dispersion and related applications', *Report No. SAND85-2806*, Sandia National Laboratories, Albuquerque, NM, 1986.
2. M. G. Marietta and W. F. Simmons, 'Subseabed disposal project annual report: ocean modeling studies. October 1983 through September 1984', *SAND86-0929*, Sandia National Laboratories, Albuquerque, NM, 1986.
3. D. B. Haidvogel, A. R. Robinson and C. G. H. Rooth, 'Eddy-induced dispersion and mixing', in A. R. Robinson (ed.), *Eddies in Marine Science*, Springer-Verlag, NY, 1983, pp. 481–491.
4. K. J. Richards, 'The interaction between the bottom mixed layer and mesoscale motions of the ocean: a numerical study', *J. Phys. Oceanogr.*, **14,** 754–768 (1984).
5. K. Bryan, 'A numerical method for the study of the circulation of the world ocean', *J. Comp. Phys.*, **4,** 347–376 (1969).
6. A. J. Semtner, 'An oceanic general circulation model with bottom topography', *NTIS PB 276 840.*
7. D. B. Haidvogel, A. R. Robinson and F. F. Schulman, 'The accuracy, efficiency and stability of three numerical models with application to open ocean problems', *J. Comp. Phys.*, **34,** 1–53 (1980).
8. R. N. Miller, A. R. Robinson and D. B. Haidvogel, 'A baroclinic quasigeostrophic open ocean model', *J. Comp. Phys.*, **50,** 38–70 (1983).
9. G. L. Weatherly and P. J. Martin, 'On the structure and dynamics of the oceanic bottom boundary layer', *J. Phys. Oceanogr.*, **8,** 557–570 (1978).
10. J. A. Carton and S. G. N. Philander, 'Coastal upwelling viewed as a stochastic process', *J. Phys. Oceanogr.*, **14,** 1499–1509 (1984).
11. T. Yamada, 'A numerical simulation of nocturnal drainage flow', *J. Meteor. Soc. Japan*, **59,** 108–122 (1981).
12. D. E. Dietrich and M. G. Marietta, 'An ocean modeling system with turbulent boundary layers and topography: general circulation results' (in preparation).
13. A. Arakawa and V. R. Lamb, 'Computational design of the basic dynamical processes of the UCLA general circulation model', *Methods in Computational Physics, Vol. 17*, Academic Press, 1977, pp. 174–265.
14. G. L. Mellor, and T. Yamada, 'Development of a turbulence closure model for geophysical fluid problems', *Reviews of Geophysics and Space Physics*, **30,** 851–875 (1982).
15. L. Rosenhead, *Laminar Boundary Layers*, Oxford University Press, 1963.
16. D. Laird and D. E. Dietrich, Personal communication, 1982.
17. P. J. Roache, *Computational Fluid Dynamics*, Hermosa Publishers, Albuquerque, NM, 1976.
18. E. Yakimiw and A. Robert, 'Accuracy and stability analysis of a fully implicit scheme for the shallow water equations', *Mon. Wea. Rev.*, **114,** 240–244 (1986).
19. D. E. Dietrich and J. J. Wormeck, 'An optimized implicit scheme for compressible reactive gas flow', *Numerical Heat Transfer*, **8,** 335–348 (1985).
20. A. Robert, 'The integration of a low order spectral form of the primitive meteorological equations', *J. Meteor. Soc. Japan*, **44,** 236–245 (1966).
21. R. Asselin, 'Frequency filter for time integrations', *Mon. Wea. Rev.*, **100,** 187–190 (1972).
22. D. E. Dietrich, 'Optimized block-implicit relaxation', *J. Comp. Phys.*, **18,** 421–439 (1975).
23. D. E. Dietrich, 'Numerical solution of fully-implicit energy conserving primitive equations', *J. Meteor. Soc. Japan*, **53,** 222–225 (1975).
24. D. E. Dietrich, 'Stabilized error vector propagation (SEVP): elliptic solvers for ocean models', *SAND85-7225*, Sandia National Laboratory, Albuquerque, NM, 1986.
25. P. J. Roache, 'Marching methods for elliptic problems', *Numerical Heat Transfer*, **1,** 1–25 (Part 1), 163–181 (Part 2) and 183–201 (Part 3) (1978).

26. G. Peggion, 'The effect of the benthic boundary layer on the physics of intense mesoscale eddies', *Ph.D. Thesis*, Florida State University, 1984.
27. A. J. Semtner, 'A numerical investigation of the arctic ocean circulation', *Ph.D. Thesis*, Princeton University, 1973.
28. K. Bryan, S. Manabe and R. C. Pacanowski, 'A global ocean–atmosphere climate model. Part II. The oceanic circulation', *J. Phys. Oceanogr.*, **5**, 30–46 (1975).
29. J. R. Holton, *An Introduction to Dynamic Meteorology*, Academic Press, NY, 1972.
30. D. E. Dietrich and N. Brunet, 'Precipitation modulation by large-scale inertia–gravity waves', *J. Meteor. Soc. Japan*, **57**, 469–473 (1979).
31. S. Steinberg and P. J. Roache, 'Symbolic manipulation and Computational fluid dynamics', *J. Comp. Phys.*, **57** (2), 251–284 (1985).
32. P. J. Roache and D. E. Dietrich, 'Evaluation of the filtered leapfrog–trapezoidal time integration method', submitted for publication in *Numerical Heat Transfer*.